Eur. Phys. J. C (2025) 85:795
https://doi.org/10.1140/epjc/s10052-025-14510-5

THE EUROPEAN PHYSICAL JOURNAL C

Regular Article - Theoretical Physics

Shadows of rotating non-commutative Kiselev black holes: constraints from EHT observations of M87* and Sgr A*

Fazlay Ahmed[1,a], **Heena Ali**[2,b], **Qiang Wu**[1,3,c], **Tao Zhu**[1,3,d], **Sushant G. Ghosh**[2,4,e]

[1] Institute for Theoretical Physics and Cosmology, Zhejiang University of Technology, Hangzhou 310023, China
[2] Centre for Theoretical Physics, Jamia Millia Islamia, New Delhi 110025, India
[3] United Center for Gravitational Wave Physics (UCGWP), Zhejiang University of Technology, Hangzhou 310032, China
[4] Astrophysics and Cosmology Research Unit, School of Mathematics, Statistics, and Computer Science, University of KwaZulu-Natal, Private Bag 54001, Durban 4000, South Africa

Received: 6 May 2025 / Accepted: 6 July 2025

Abstract The Event Horizon Telescope (EHT) imaged black holes M87* (angular diameter $\theta_d = 42 \pm 3\,\mu$as, mass $\sim 6.5 \times 10^9\, M_\odot$) and Sgr A* ($\theta_d = 48.7 \pm 7\,\mu$as, shadow deviation $\delta \approx -0.08^{+0.09}_{-0.09}$ (VLTI), $-0.04^{+0.09}_{-0.10}$) (Keck). These observations enable tests of gravity in strong regimes. We propose a rotating non-commutative inspired Kiselev black hole (RNKBH), incorporating dark energy (ω) and non-commutative (Θ) parameters, extending Kerr solutions. Our analysis reveals that $\omega = -2/3$ allows larger Θ but requires $a \geq 0.16M$ to maintain horizons. Shadow calculations show significant deviations from Kerr predictions: for $\Theta = 0.001 - 0.005M^2$, shadows shrink by 8-15% and distortion increases by 20-35% for rapidly spinning ($a > 0.5M$) black holes. The $\omega = -2/3$ exhibits shadow squeezing near the cosmological horizon. We compute shadow observables and compare them with EHT data. For Sgr A* (50° inclination), the bounds are $0.001497 \leq \Theta \leq 0.002868\, M^2$ at $a = 0.9146$ ($\omega = -2/3$). For M87* (17°), $0 \leq \Theta \leq 0.004993\, M^2$ at $a = 0.0.6167$ ($\omega = -2/3$). While EHT cannot yet distinguish RNKBH from Kerr BH, our results highlight its viability as an astrophysical candidate.

1 Introduction

Significant progress has been made in the study of black holes in recent years, particularly after the groundbreaking detection of gravitational waves by LIGO [1–3]. Further, the recent advancements in very long baseline interferometry (VLBI) have opened unprecedented avenues for probing the immediate vicinity of supermassive black holes (SMBHs). Observations by the Event Horizon Telescope (EHT) of the SMBHs M87* [4–6] and SgrA* [7,8] have provided direct imaging of their shadows, offering a crucial testing ground for the predictions of general relativity (GR) and modified theories of gravity in the strong-field regime. These observations allow the extraction of critical black hole parameters and impose stringent constraints on various modified gravity models and exotic compact objects. The EHT's results on M87* and Sgr A* have spurred discussions about their implications for GR, specifically whether such results can effectively test deviations from GR in strong-gravity environments [9,10]. Methodologies such as variational image feature extraction [11] and general relativistic radiation transport models [12] have been instrumental in analyzing these observations. Additionally, constraints on black hole charge and departures in metric properties have been considerably studied [13,14], further enhancing our understanding of SMBH environments. The theoretical framework for calculating the shadow of black holes has garnered a lot of attention in recent decades, thanks to the groundbreaking work of Synge [15] and Luminet [16], who developed the expression for the angular radius of the photon capture region surrounding the Schwarzschild black hole. Black hole shadows provide a rich observational framework for testing alternative theories of gravity, as deviations from the Kerr metric may leave detectable imprints on the shadow's morphology. Efforts to test Horndeski gravity [17], Einstein–Gauss–Bonnet gravity [18], and massive gravity [19] have leveraged EHT constraints to validate or constrain these theories. Moreover,

[a] e-mail: fazleyamuphysics@gmail.com
[b] e-mail: Heenasalroo101@gmail.com
[c] e-mail: wuq@zjut.edu.cn (corresponding author)
[d] e-mail: zhut05@zjut.edu.cn
[e] e-mail: sghosh2@jmi.ac.in

Published online: 23 July 2025

studies focusing on rotating black hole metrics and horizonless objects have broadened the scope of gravitational tests [20,21]. The study of black hole shadows has become a pivotal tool for probing near-horizon geometries, driving extensive research within the framework of GR [22–40]. Beyond GR, shadows have been extensively analyzed in modified theories of gravity (MTGs) [17,35,37,41–67]. The inclusion of extra dimensions in modified gravitational frameworks has further broadened the scope of shadow studies to higher-dimensional spacetimes [44,45,48,53,68–73]. Black hole shadows are particularly significant for testing strong-field gravitational effects and evaluating the validity of the no-hair theorem [17,35,74–81]. Ghosh and Afrin [82] used shadow morphology to constrain Sgr A*'s charge, highlighting EHT data's role in linking observations with fundamental physics.

Among the alternative models, black holes surrounded by quintessence [83] and non-commutative geometries [84] provide intriguing scenarios to investigate deviations from the Kerr metric. While widely interpreted as describing a black hole surrounded by quintessence, the Kiselev metric is not sourced by a perfect fluid or a canonical scalar field. As shown in Visser's paper [85], the stress-energy tensor corresponds to an anisotropic fluid with unequal radial and tangential pressures. The term "quintessence" in this context is thus used in a phenomenological sense, reflecting the energy density's radial fall-off behaviour similar to that expected from dark energy-like components. Although commonly referred to as a black hole surrounded by 'quintessence,' the Kiselev solution, in fact, arises from an anisotropic fluid source, not a perfect fluid or scalar field, as emphasized by Visser [85]. We adopt the term 'quintessence' in a phenomenological sense, consistent with much of the existing literature.

The influence of exotic fields such as quintessence on black hole shadow, deflection angle, and lensing effects has been explored in various theoretical contexts, demonstrating their potential to affect SMBH observables [86,87]. Furthermore, incorporating quantum effects into black hole metrics, such as loop quantum gravity and quantum-corrected models, has also attracted significant attention in light of EHT observations [80,81,81,88–93]. Recent works have further scrutinized the role of accretion dynamics and magnetic fields in shaping the observational characteristics of black hole shadows. Studies have highlighted the importance of accretion turbulence and multi-wavelength analyses in constraining black hole parameters [94,95]. Additionally, lensing and greybody factors, particularly for rotating and charged black holes, have provided complementary insights into the nature of SMBHs [96–98]. The motivation for this study lies in the interplay between theoretical advancements and observational constraints. MTGs, such as those inspired by non-commutative geometry, often predict deviations in shadow morphology, horizon structure, and lensing effects [82,99]. Including quintessence, a candidate for dark energy, further complicates the dynamics around black holes, necessitating precise observational tests to discern its influence [100,101]. The EHT observed Images of M87* and Sgr A* have been used to constrain deviations from GR, such as in Einstein–Æther theory [64], and Lorentz-violating extensions of the Standard Model [65]. The effects of exotic environments, like axion-plasmon clouds, on black hole shadows have also been explored [66]. Notably, EHT data has ruled out compact objects in baseline mimetic gravity [67]. This paper aims to investigate the shadows of rotating non-commutative inspired Kiselev Black Holes (RNKBH), incorporating the EHT observations of M87* and Sgr A* as constraints. We analyze the deviations in shadow morphology induced by these exotic effects and explore the compatibility of theoretical predictions with EHT data. By considering recent studies on dynamical torsion, non-linear electrodynamics, and higher-dimensional theories [102–104], we provide a comprehensive analysis of black hole shadows under modified gravity frameworks.

The structure of this paper is as follows: Sect. 2 introduces the theoretical framework, detailing the non-commutative inspired rotating black hole metric and its coupling to quintessence. Section 3 outlines the methodology for calculating black hole shadows using the null geodesic equations and the vital observational constraints from EHT data. Section 4 presents our results, comparing shadow characteristics across various parameter regimes. Section 5 is dedicated to estimating the parameters associated with black holes using two widely recognized techniques. Section 6 explores how EHT observations constrain black hole parameters. Finally, Sect. 7 discusses the implications of our findings for future theoretical and observational studies.

2 Rotating non-commutative Kiselev back holes

Kiselev [105] introduced the principle of additivity and linearity in the energy–momentum tensor, allowing for consistent recovery of known limits such as the electromagnetic field and de Sitter spacetime. This formulation provides a relativistic relation between energy density and pressure. Within this framework, he obtained a static, spherically symmetric black hole solution surrounded by quintessence. Following this idea, various extensions and related black hole solutions have been proposed [63,83,83,106–114]. Inspired by Kiselev's approach, we aim to derive a black hole solution in a non-commutative geometry-inspired spacetime. We start with a general static, spherically symmetric metric:

$$ds^2 = -f(r,\omega)dt^2 + \frac{1}{f(r,\omega)}dr^2 + r^2 d\Omega^2, \tag{1}$$

where the function $f(r)$ is expressed as

$$f(r,\omega) = 1 - \frac{2M}{r} - \frac{c}{r^{3\omega+1}}. \tag{2}$$

Here M is the black hole mass, ω is a quintessential equation of state parameter with a range $-1 < \omega < -1/3$, and c is a positive normalization factor given by

$$\rho_q = -\frac{c}{2}\frac{3\omega}{r^{3(1+\omega)}}, \tag{3}$$

where ρ_q is the density of quintessence. Moreover, Eq. (3) explicitly implies that $\rho_q > 0$, which in turn requires $cw < 0$. Since $c > 0$, it follows that $w < 0$. The metric (1) encompasses the Schwarzschild black hole without the normalization factor c. In a commutative space-time, the mass density of a point particle is defined as the product of its mass and a Dirac delta function [115].

The noncommutative-inspired model offers potential insights into the nature of gravity, as noncommutative geometry inherently introduces the smearing of matter distributions. In this theory, spacetime coordinates are treated as operators due to an inherent uncertainty captured by the commutation relation

$$[x_a, x_b] = i\theta_{ab},$$

with θ_{ab} is a 4×4 antisymmetric matrix that characterises the fundamental discretisation scale of spacetime. This relation leads to a GUP of the form

$$\Delta x^\mu \Delta x^\nu \geq \frac{1}{2}|\theta^{\mu\nu}|. \tag{4}$$

This framework can be viewed as a refinement of semiclassical gravity, providing a pathway to incorporate noncommutative effects, which remain elusive in a fully developed theory. This idea was realised by Nicolini et al. [116] to propose one of the first noncommutative geometry-inspired Schwarzschild black holes, which is an exact solution from the Einstein equations for the static, spherically symmetric, Gaussian-smeared matter source.

It looks improper due to the natural fuzziness of space caused by the uncertainty relation [115]. In this regard, the non-commutative parameter Θ, which is a small positive number, should measure the fuzziness. Various types of mass densities have been recommended in the literature [117–122]. In this work, we used the following distribution form [118]:

$$\rho_\Theta(r) = \frac{M\sqrt{\Theta}}{r^{3/2}(r^2+\pi\Theta)^2}. \tag{5}$$

In this case, the mass distribution leads to

$$\begin{aligned} M(r,\Theta) &= 4\pi\int^r r^2\rho_\Theta(r)dr \\ &= \frac{2M}{\pi}\left[\tan^{-1}\left(\frac{r}{\sqrt{\pi\Theta}}\right) - \frac{r\sqrt{\pi\Theta}}{r^2+\pi\Theta}\right]. \end{aligned} \tag{6}$$

The first-order correction in the non-commutative term can be rewritten as

$$M(r,\Theta) \approx M - \frac{4M}{\sqrt{\pi}r}\sqrt{\Theta}. \tag{7}$$

Consequently, it is made clear that a particle's mass is not confined at a point in the non-commutative spacetime. However, it is supposed to be distributed throughout the region with a linear size of $\sqrt{\Theta}$. We use this fact to reformulate the Kiselev black hole solution by interchanging the smeared mass distribution with the ordinary mass term:

$$f(r,\omega,\Theta) = 1 - \frac{2M}{r} + \frac{8M}{\sqrt{\pi}r^2}\sqrt{\Theta} - \frac{c}{r^{3\omega+1}}. \tag{8}$$

Since rotation plays an important role in defining the geometry of a black hole in GR and MTG, our interest is shifted towards the rotating solution of the metric (1). The Newman–Janis algorithm (NJA) [123] is such a framework for developing the rotating solution. We employed the aforementioned approach for metric (1) and derived the stationary and axisymmetric counterpart of the spherically symmetric solution characterized by parameters M, a, Θ, c, and ω in the Boyer–Lindquist coordinates, which reads

$$\begin{aligned} ds^2 = &-\left[\frac{\Delta - a^2\sin^2\theta}{\Sigma}\right]dt^2 \\ &- 2a\sin^2\theta\left[1 - \frac{\Delta - a^2\sin^2\theta}{\Sigma}\right]dtd\phi \\ &+ \sin^2\theta\left[\Sigma + a^2\sin^2\theta\left(2 - \frac{\Delta - a^2\sin^2\theta}{\Sigma}\right)\right]d\phi^2 \\ &+ \frac{\Sigma}{\Delta}dr^2 + \Sigma d\theta^2, \end{aligned} \tag{9}$$

with

$$\begin{aligned} \Delta &= r^2 + a^2 - 2Mr + \frac{8M\sqrt{\Theta}}{\sqrt{\pi}} - \frac{c}{r^{3\omega-1}}, \\ \Sigma &= r^2 + a^2\cos^2\theta, \end{aligned} \tag{10}$$

where a is the angular momentum. The non-commutative parameter Θ and the normalization factor c offer a potential deviation of metric (9) from the standard Kerr black holes. For definiteness, the metric (9) is termed as Rotating Noncommutative Inspired Kiselev Black Hole (RNKBH), which encompasses the Kerr black hole when Θ and c are equal to zero. Our main focus in this work is to explore the impact of the non-commutative parameter Θ and the quintessential

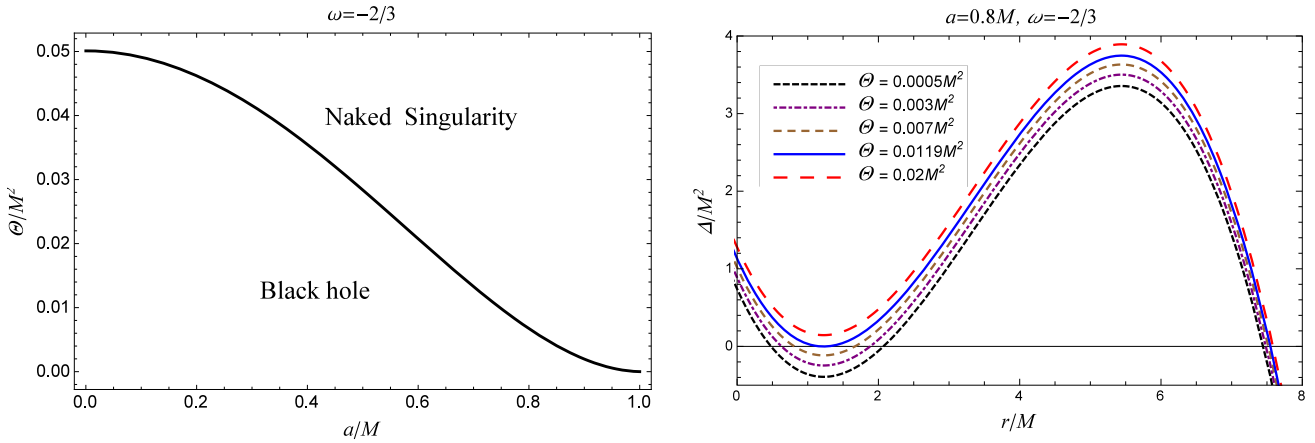

Fig. 1 The parameter space $(a/M - \Theta/M^2)$ (left) and the horizons (right) of the RNKBHs for $\omega = -2/3$. The extremal black holes are represented by the black curve and the blue curve, respectively

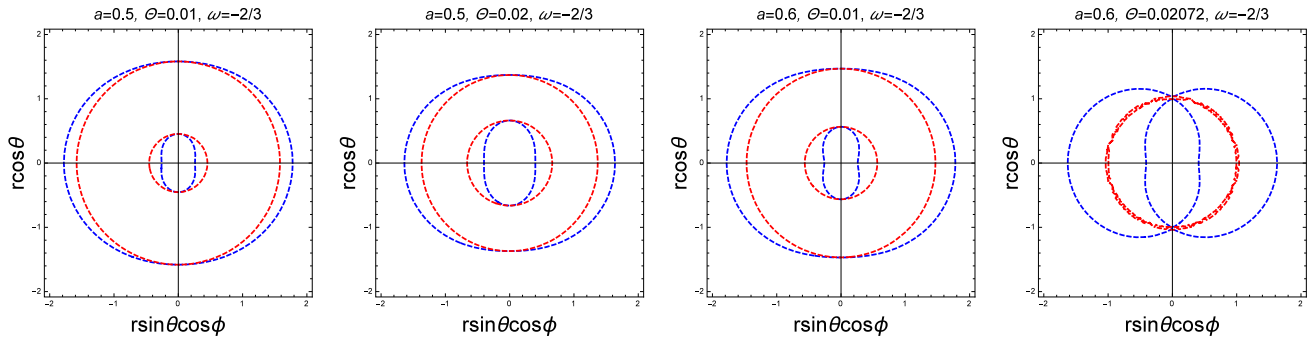

Fig. 2 The cross-section of EH (outer red curve), SLS (outer blue curve) and ergoregion of the RNKBHs

equation of the state parameter ω on the horizon structure and shadows.

The metric (9) is singular at space-time points where $\Sigma \neq 0$ and $g^{\mu\nu}\partial_\mu r \partial_\nu r = g^{rr} = \Delta = 0$. Although this singularity is coordinate dependent and can be eliminated by the appropriate choice of coordinates, in contrast, the singularity $r = 0$ is an artifact of GR and a curvature singularity. The location of the horizons is determined by the condition $\Delta = 0$ as

$$r^2 + a^2 - 2Mr + \frac{8M\sqrt{\Theta}}{\sqrt{\pi}} - \frac{c}{r^{3\omega-1}} = 0. \tag{11}$$

The roots of Eq. (11) indicate black hole horizons: the event horizon (r_+) and the Cauchy horizon (r_-). We analyze the specific case of $\omega = -2/3$ (quintessence). Uniquely, for $\omega = -2/3$, three horizons (Cauchy, event, and cosmological) appear when $\Theta \leq 0.0119$. The outermost is the cosmological horizon, marking the observable universe's edge. The extremal case defines bounds on Θ and a. Figure 1 (left) shows the parameter space separating black hole and naked singularity regions, suggesting that small Θ allows larger a and that Θ must remain small. The Fig. 1 (right) also illustrates how ω and Θ influence horizon formation, with the $\omega = -2/3$ notably yielding three horizons.

An additional surface, the static limit surface, lies outside the event horizon where the asymptotic time-translation Killing vector $\chi^i = (\partial/\partial t)^i$ becomes null, i.e.,

$$\chi^i \chi_i = g_{tt} = r^2 + a^2\cos^2\theta - 2Mr + \frac{8M\sqrt{\Theta}}{\sqrt{\pi}} - \frac{c}{r^{3\omega-1}} = 0. \tag{12}$$

The largest root of Eq. (12) marks the outer static limit surface. For fixed a, Θ, and θ, it defines the extremal boundary of this surface. The region between the event horizon and the static limit surface is the ergoregion (Fig. 2), where χ^i becomes space-like, forcing any observer to co-rotate with the black hole. Increasing Θ enlarges the ergoregion, making the RNKBH's ergoregion larger than that of a standard Kerr black hole. Moreover, higher Θ and rapid rotation can lead to disconnected horizons. The ergoregion is significant due to its role in energy extraction via the Penrose process [124].

3 Geodesics around rotating black holes

The black hole shadow is shaped by photon orbits, which makes it essential to study photon motion in the given spacetime. Since the metric (9) is independent of t and ϕ, it admits Killing vectors $\chi^{\mu}_{(t)} = \delta^{\mu}_{t}$ and $\chi^{\mu}_{(\phi)} = \delta^{\mu}_{\phi}$, leading to conserved quantities: energy $E = -p_t$ and axial angular momentum $L_z = p_\phi$. For photons ($m_0 = 0$), a third conserved quantity, the Carter constant $\mathcal{Q}$, arises from hidden symmetries [125]. The Hamilton–Jacobi method is used to derive first-order geodesic equations [125,126].

$$\Sigma\frac{dt}{d\lambda} = \frac{r^2+a^2}{\Delta}(E(r^2+a^2) - aL_z) - a(aE\sin^2\theta - L_z), \tag{13}$$

$$\Sigma\frac{d\phi}{d\lambda} = \frac{a}{\Delta}(E(r^2+a^2) - aL_z) - (aE - \frac{L_z}{\sin^2\theta}), \tag{14}$$

$$\Sigma\frac{dr}{d\lambda} = \pm\sqrt{\mathcal{R}(r)}, \tag{15}$$

$$\Sigma\frac{d\theta}{d\lambda} = \pm\sqrt{\Theta(\theta)}, \tag{16}$$

where λ is the affine parameter along the geodesics, and the effective potentials $\mathcal{R}(r)$ and $\Theta(\theta)$ for radial and polar motion are given by

$$\mathcal{R}(r) = E^2\left[\left((r^2+a^2) - a\xi\right)^2 - \Delta\left(\eta + (a-\xi)^2\right)\right], \tag{17}$$

$$\Theta(\theta) = E^2[\eta - \left(\frac{\xi^2}{\sin^2\theta} - a^2\right)\cos^2\theta], \tag{18}$$

where η and ξ are dimensionless impact parameters given by

$$\xi = \frac{L_z}{E}, \quad \eta = \frac{\mathcal{K}}{E^2}. \tag{19}$$

The impact parameters reduce the degrees of freedom, with the Carter constant related via $\mathcal{Q} = \mathcal{K} + (aE - L_z)^2$ [126]. Photon motion is allowed where $\mathcal{R}(r) \geq 0$ and $\Theta(\theta) \geq 0$, with turning points at $\mathcal{R}(r) = 0$ or $\Theta(\theta) = 0$. Photons near a black hole may escape, be trapped, or follow unstable circular orbits. The latter, corresponding to peaks in the radial potential, determine the shadow boundary [126,127]. These orbits satisfy:

$$\mathcal{R} = \mathcal{R}' = 0, \quad \mathcal{R}'' \leq 0. \tag{20}$$

Solving Eq. (20) results in the critical impact parameters $(\xi_{crit}, \eta_{crit})$ of the unstable circular orbits,

$$\xi_{crit} = \frac{(a^2+r^2)\Delta'(r) - 4r\Delta(r)}{a\Delta'(r)},$$

$$\eta_{crit} = \frac{r^2\left(8\Delta(r)\left(2a^2 + r\Delta'(r)\right) - r^2\Delta'(r)^2 - 16\Delta(r)^2\right)}{a^2\Delta'(r)^2}, \tag{21}$$

where $'$ stands for the derivative with respect to the radial coordinate. Equation (21) yields the critical impact parameter for the Kerr black hole in the limit $\Theta \to 0$ [31]. Unstable photon orbits have been extensively studied for black holes and naked singularities [128–133]. In axisymmetric spacetimes, there are two types of unstable circular orbits: prograde (co-rotating) and retrograde (counter-rotating). Due to frame dragging, retrograde photons follow wider orbits to compensate for reduced angular momentum [133–135]. Photons remain in planar orbits if $\eta_{\text{crit}} = 0$, while nonplanar orbits arise for $\eta_{\text{crit}} > 0$. The radii of prograde (r_p^-) and retrograde (r_p^+) orbits are obtained from the zeros of $\eta_{\text{crit}} = 0$.

4 Shadows of RNKBHs

The black hole shadow is the dark silhouette formed by light bending around a black hole due to gravitational lensing and photon capture near the event horizon [41,50,58,136–142]. Its formation depends on the black hole's geometry, lensing effects, and the event horizon that traps light. The shadow offers indirect evidence of a black hole and insights into its properties, such as mass, spin, charge, and possible deviations from GR [28–30,35,143–145]. Its shape and size vary with parameters like inclination angle, observer distance, and spacetime geometry. Assuming an isotropic light source distribution, photons orbit, scatter, or are trapped, forming the shadow seen by a distant observer at inclination i. The shadow boundary is described using celestial coordinates X and Y [31] given by

$$X = \lim_{r_o\to\infty}\left(-r_o^2\sin i\frac{d\phi}{dr}\right),$$
$$Y = \lim_{r_o\to\infty}\left(r_o^2\frac{d\theta}{dr}\right), \tag{22}$$

where r_0 is the distance between the black hole and the observer. For a distant viewer, Eq. (22) leads to

$$X = -\xi_{crit}\csc i,$$
$$Y = \pm\sqrt{\eta_{crit} + a^2\cos^2 i - \xi_{crit}^2\cot^2 i}. \tag{23}$$

Further, if the viewer is on the equatorial plane ($i = \pi/2$), the above equation simplifies to

$$X = -\xi_{crit},$$
$$Y = \pm\sqrt{\eta_{crit}}. \tag{24}$$

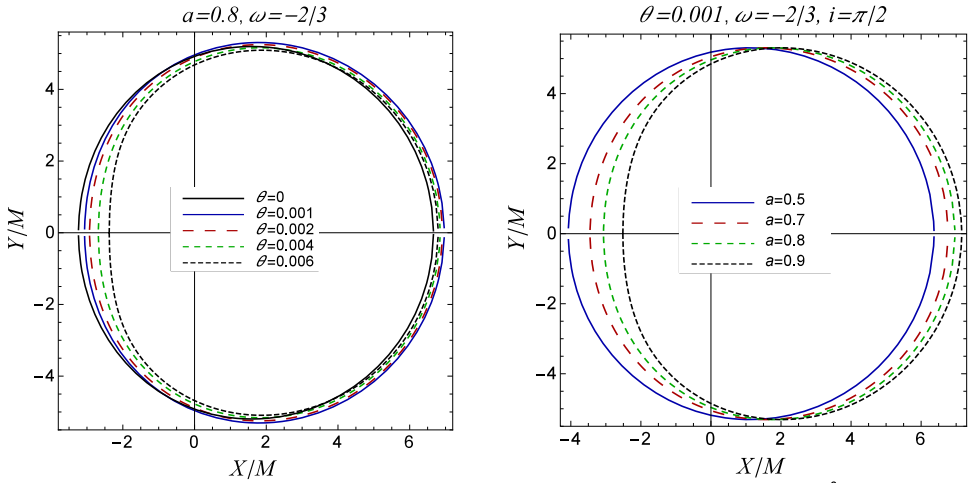

Fig. 3 Shadows of RNKBHs for fixed a and varying Θ (left), compared with the Kerr black hole ($\Theta = 0$) and fixed Θ and varying a (right). The inclination angle is $i = 90^0$

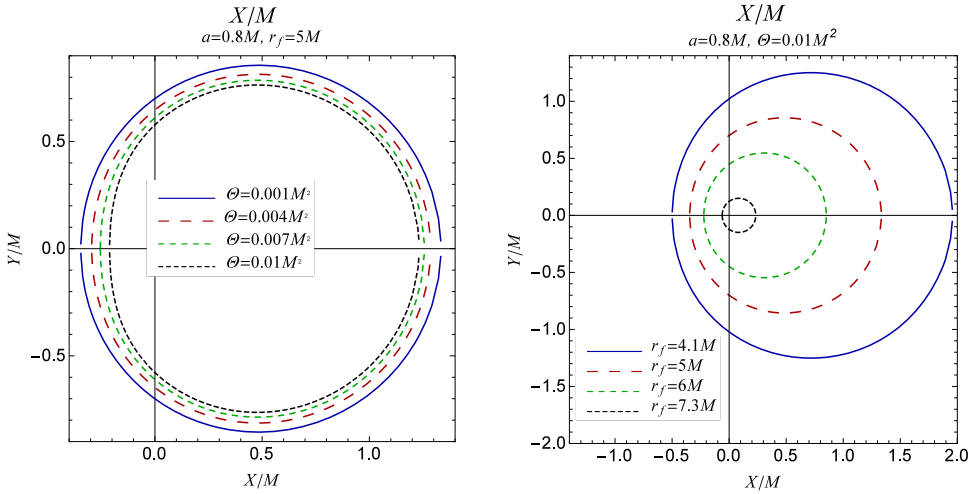

Fig. 4 Shadows for RNKBHs for a stationary observer at a finite distance (left), and a moving observer (right) for $\omega = -2/3$

The contour of X and Y outlines the shadow for the RNKBH. Equation (24), on using metric (1), yields

$$X = -\left.\frac{[a^2-3r^2]M(r)+r[a^2+r^2][1+M'(r)]}{a[M(r)+r[-1+M'(r)]]}\right|_{r=r_p},$$

$$Y = \pm\frac{1}{a[M(r)+r[-1+M'(r)]]}\Big[r^{3/2}\Big[-r^3(1+M'(r)^2) + M(r)[4a^2+6r^2-9rM(r)]-2r[2a^2+r^2 - 3rM(r)]M'(r)\Big]^{1/2}\Big]\Big|_{r=r_p}, \quad (25)$$

Equation (25) is applicable for computing the shadow for a general value of ω. However, in the presence of an additional de Sitter horizon, it is no longer valid and requires a separate treatment, as demonstrated below. The shadow size is significantly influenced by the non-commutative parameter Θ.

4.1 Case $\omega = -2/3$

For $\omega = -2/3$, the spacetime admits cosmological, event, and Cauchy horizons. The cosmological horizon limits visibility, so shadows can only be observed within a specific range. The observer must lie between the photon sphere and the cosmological horizon. To meet this condition, we follow the method in [143], where celestial coordinates ϕ and ψ are defined accordingly.

$$\sin\Psi(r_f,r_p) = \left.\left(\frac{\xi_{crit}-a}{\sqrt{(a-\xi_{crit})^2+\eta_{crit}}}\right)\right|_{r=r_f},$$

$$\sin\Phi(r_f,r_p) = \left.\left(\frac{\sqrt{\Delta[(a-\xi_{crit})^2+\eta_{crit}]}}{(r^2+a^2-a\xi_{crit})}\right)\right|_{r=r_f}. \quad (26)$$

To project the shadow on a plane, we introduce the Cartesian coordinates,

$$X(r_f,r_p) = -2\tan\left(\frac{\Phi(r_f,r_p)}{2}\right)\sin(\Psi(r_f,r_p)),$$

$$Y(r_f,r_p) = -2\tan\left(\frac{\Phi(r_f,r_p)}{2}\right)\cos(\Psi(r_f,r_p)), \quad (27)$$

which satisfy the following relation

$$X^2+Y^2 = 4\tan^2\left(\frac{\Phi(r_f,r_p)}{2}\right). \quad (28)$$

The contour plot of $X(r_f,r_p)$ vs. $Y(r_f,r_p)$ in Eq. (27) illustrates the shadow of a rotating black hole surrounded by quintessence (cf. Fig. 3). In Fig. 4, we show shadow variations for stationary and moving observers. For a stationary

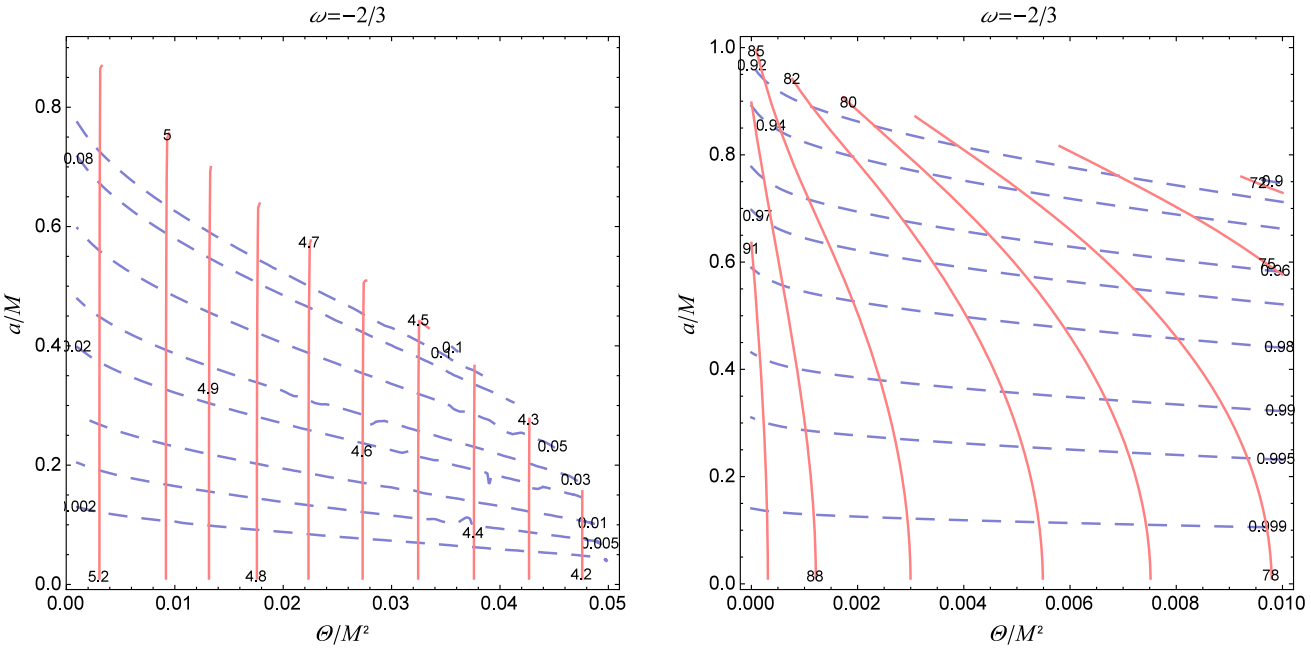

Fig. 5 Contour plots of the observables R_s/M, δ_s (left) and A/M^2, D (right) in RNKBH parameter space $(a/M, \Theta/M^2)$. Constant R_s/M and A/M^2 are represented by solid red curves, while constant δ_s and D are represented by dashed blue curves respectively

observer at $r = 5M$, the shadow size decreases with increasing non-commutative parameter Θ. For a moving observer, the shadow's size and distortion vary with position: it grows and distorts near the event horizon, leading to darkness, while it shrinks to a point near the cosmological horizon, where the observer sees a fully illuminated sky.

5 Observables and black hole parameter estimation

Various spacetime parameters affect black hole shadows, as seen in Figs. 3 and 4. Shadow analysis helps test gravity theories and assess parameter effects [30,35,37,47,49,58,77,146–150]. In this work, we study shadows on the RNKBH background, constraining parameters using *EHT* data. Although M87* and Sgr A* images align with Kerr predictions, they also motivate the exploration of alternatives in modified gravity [4–6]. To match theory with observation, we estimate parameters, focusing on the equatorial plane (90°) where distortion is maximal. Two frequently used techniques are employed for this purpose:

a. Hioki and Maeda method: Hioki et al. [31] defined two observables, R_s and δ_s, to characterize black hole shadow size and distortion. R_s represents the radius of a reference circle while δ_s measuring the difference between the left edge of the shadow and the boundary of the circle. The reference circle aligns with the top, bottom, and right edges of the shadow, while intersections with the leftmost shadow edge and the horizontal axis define the observables [151]. R_s approximates the shadow size and δ_s reflects the deviation from the reference circle.

$$R_s = \frac{(X_t - X_r)^2 + Y_t^2}{2|X_r - X_t|}, \tag{29}$$

using the relations $X_b = X_t$ and $Y_b = -Y_t$, and

$$\delta_s = \frac{|X_l - X_l^{'}|}{R_s}, \tag{30}$$

where subscripts r, l, t, and b, respectively, stand for the right, left, top, and bottom of the shadow boundary.

The shadow size and shape are significantly influenced by the parameter Θ. Using the method of Hioki and Maeda [31], we estimated the size of the shadow and examined the effects of Θ and a. The shadow radius R_s of an RNKBH decreases as Θ increases and is smaller for large a and Θ. The distortion δ_s is inversely proportional to R_s, growing with larger a and Θ. To quantify the parameters, we plotted R_s and δ_s in the $(\Theta/M^2 - a/M)$ space (Fig. 5), where the red and blue lines intersect, providing the quantitative analysis in Table 1.

b. Kumar and Ghosh method: The Hioki and Maeda method [31] for black hole parameter analysis using R_s and δ_s was extended by Tsupko [152] for analytical estimation, and Tsukamoto [153] differentiated Kerr black holes in modified gravity. However, these observables may not apply to irregular shadows in modified gravity [142,153,154], and noisy data can distort shape [27,29]. To address this, Kumar and Ghosh [29] introduced oblateness (D) and shadow area (A)

Table 1 Estimated values of RNKBH parameters of a/M and Θ/M^2 using the shadow observables R_s and δ_s for $\omega = -2/3$ at inclination angle of $i = 90°$

R_s/M	δ_s	Θ/M^2	a/M
5.2	0.1	0.003039	0.726
5.0	0.08	0.009179	0.591
4.9	0.1	0.01327	0.589
4.8	0.05	0.01769	0.4208
4.6	0.08	0.02728	0.4227
4.5	0.01	0.03245	0.1546

Table 2 Estimated values of RNKBH parameters of a/M and Θ/M^2 using the shadow observables A/M^2 and D for $\omega = -2/3$ at an inclination angle of $i = 90°$

A/M^2	D	Θ/M^2	a/M
88	0.99	0.000873	0.3999
85	0.98	0.00188	0.5256
82	0.98	0.00407	0.4952
80	0.97	0.005186	0.5733
78	0.99	0.008908	0.3305

defined by

$$A = 2\int Y(r_p)dX(r_p) = 2\int_{r_p^-}^{r_p^+}\left(Y(r_p)\frac{dX(r_p)}{dr_p}\right)dr_p, \tag{31}$$

and

$$D = \frac{X_r - X_l}{Y_t - Y_b}. \tag{32}$$

In the case of a non-rotating black hole ($a = 0$), $D = 1$, and for an extremal Kerr black hole ($a = M$), $D = \sqrt{3}/2$. For an equatorial observer, the oblateness D falls within the range $\sqrt{3}/2 \leq D < 1$ [152]. For given a and Θ, both A and D decrease with a and Θ. We plotted the contour diagram of the observables A and D in the parameter space of $(\Theta/M^2 - a/M)$, depicted in Fig. 5. The red and blue lines indicate the contours of A and D that intersect at some specified points. The intersection of contours provides the estimated numerical values of a and Θ. In Table 2, the quantitative analysis of parameters a and Θ has been depicted for shadow observables A and D.

6 Constraints from EHT observations of M87* and SgrA*

The *EHT* collaboration used VLBI to capture an event horizon-scale image of the supermassive black hole M87* [4–6], offering new opportunities to test gravity. The image of M87* is nearly circular, with an angular size of $42 \pm 3\,\mu$as [4]. This aligns with the predicted image of a Kerr black hole, providing a basis for testing alternative gravity theories. We aim to set bounds on parameters for RNKBH models of M87* and SgrA* using shadow angular diameter θ_d and Schwarzschild shadow deviation δ. The angular diameter θ_d is given by $\theta_d = 2\frac{R_a}{d}$, where R_a is the shadow radius and d is the distance to the celestial plane. The shadow diameter is influenced by the black hole mass, inclination angle i, and underlying geometry parameters. Additionally, δ quantifies the difference between the shadow angular diameters of a given black hole model and the Schwarzschild black hole. The observable δ is defined as [8,155]

$$\delta = \frac{\theta_d}{\theta_d, sch} - 1. \tag{33}$$

Hence, it facilitates a clear understanding that if the shadow angular diameter of a given black hole is smaller (larger) than that of a Schwarzschild black hole with the same mass, then δ will yield a negative (positive) value. For example, in the case of a Kerr black hole, $\delta \in [-0.075, 0]$ [8], with the limits of $a \in [0, M]$ and $i \in [0, \pi/2]$. So far, if δ is bounded by the aforementioned limit for a specific model of a black hole, then its shadow aligns with the Kerr black hole. In the current work, we ascertain the values of δ for M87* and SgrA* with the help of *EHT* results. Another thing that should be noted in the current analysis is the potential for measurement uncertainties caused by the large array of telescopes, and one of them results from uncertain radiative and accretion physics [9], which obscures the actual predictions of the *EHT*. Despite these challenges, the theoretical analysis addresses the limits of *EHT* observations. The essence of non-commutative spacetime can be explored with it, and in the near future, we will be able to estimate the parameters more accurately.

*a. Bounds on M87**

In the shadow image of M87*, relativistic jets have been detected, which may be the consequence of magnetohydrodynamic exchange between rotating black holes and accretion disks. Considering the positioning of these jets in M87*, the inclination angle is estimated to be 17° concerning the observer's line of sight [156]. However, the exact measurement of the mass of M87* using independent techniques remains unresolved [148]. Taking into account the $\leq 10\%$ offset between the diameter of the ring and the photon ring, the angular diameter of the M87* shadow can be calibrated to $\theta_{sh} = 37.8 \pm 2.7\,\mu$as [157,158]. The error $\pm 2.7\%$ incorporates both measurement uncertainty and potential offset. We calculate the angular diameter of the M87 * shadow, which, in addition to a, Θ, and i, depends on the black hole mass M and the distance d. The current assessment uses the GR Kerr model and adopts the black hole's mass $M \sim 6.5 \times 10^9 M_\odot$ and distance $d = 16.8$ Mpc. We omitted measurement uncer-

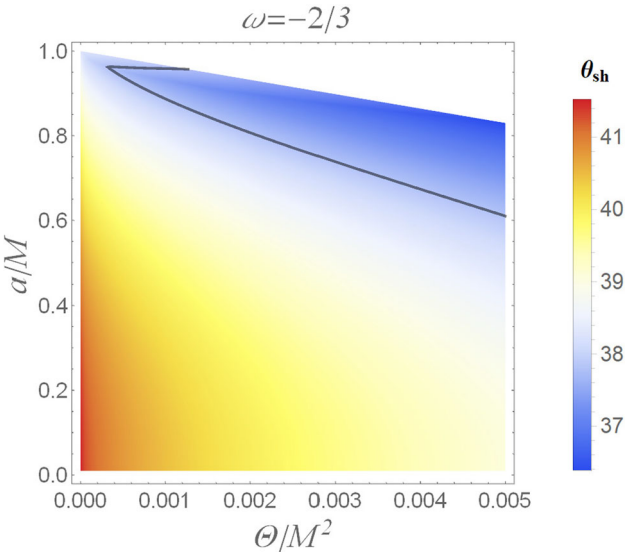

Fig. 6 The angular diameter θ_{sh} of RNKBH shadows is shown as a function of a/M and Θ/M^2 for an inclination angle of $i = 17°$. The black solid curve indicates $\theta_{sh} = 37.8\mu$as of the M87*. The white region is forbidden for $(a/M, \Theta/M^2)$

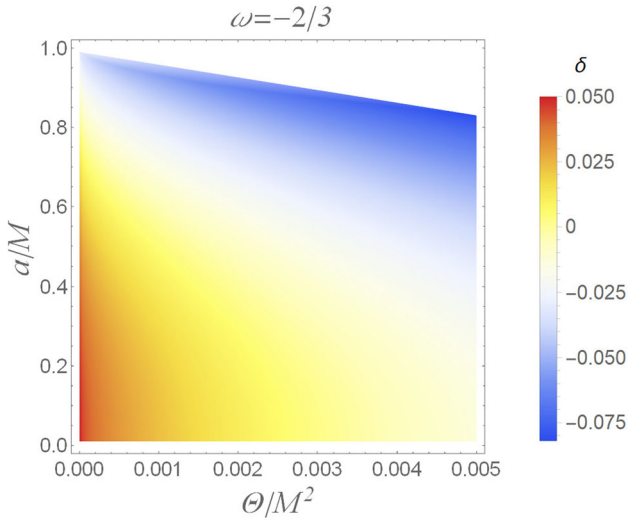

Fig. 7 Schwarzschild shadow deviation δ of RNKBH as a function of parameters a/M and Θ/M^2, with an inclination angle, $i = 17°$. The entire parameter space is in agreement with the EHT inferred value $\delta_{M87^*} = -0.01 \pm 0.17$. The white region is forbidden

tainties of mass and distance for ease, as the *EHT* observations have already included them. The shadow angular diameter $\theta_d = 2R_a/d$ for the RNKBH has been calculated and displayed in Fig. 6 as a function of a and Θ with the inclination angle of $i = 17°$. To establish bounds on $(a/M, \alpha/M^2)$, we adopt a conservative approach, considering the median value of θ_{sh} up to the maximum allowed by the RNKBH model [159]. Specifically, we select $\theta_{sh} \geq 37.8\,\mu$as indicated by the black curve. The region enclosed by it represents the parameter space $(a/M - \Theta/M^2)$ consistent with the observational results of M87*. We quantitatively computed the bounds for the shadow angular diameter of M87*. It is evident from Fig. 6 that a considerable part of $(a/M, \Theta/M^2)$ parameter space is consistent with the EHT results for M87*, and we retrieve the bounds mentioned in Table 3.

The subsequent step is to determine the Schwarzschild shadow deviation for M87*. Calibrating the shadow size of M87* with the ring diameter, which *EHT* has recorded, offers the bound at $\delta = -0.01 \pm 0.17$ [6,13]. We computed δ for M87* under the assumption of a RNKBH with an inclination angle of $i = 17°$ and represent it in Fig. 7. It is apparent that for all values of ω, the whole parameter space is satisfied with the observational result of M87*. Interestingly, from Fig. 7, we noticed that the values of $\delta < -0.075$ and $\delta > 0$ are also present there, which lie outside the expected range of the Kerr black hole. Therefore, our current analysis supports the non-Kerr model.

*b. Bounds on SgrA**

Next, we consider the RNKBH as a model for the supermassive black hole SgrA*. Unlike M87, the image of Sgr A* was more challenging to produce because of its smaller size and rapid variability. Gas orbits Sgr A* in just a few minutes, causing changes in the emitted radiation on timescales comparable to the observation. After applying some independent stellar dynamic observations from the orbits of the S0-2 star by VLTI and Keck telescopes [8,160–162], the mass of the supermassive black hole has been estimated as $M = 4.0^{+1.1}_{-0.6} \times 10^6 M_\odot$ and the distance from Earth is chosen as $d = 8$ kpc [8,155]. The average angular diameter of the shadow has been reported within the range of $46.9-50\,\mu$as, and the possibility of an inclination angle $i > 52°$ has been ruled out [8]. Interestingly, there is some precedence of the SgrA* shadow image over M87*, as it offers curvature 10^6 times higher. Numerous imaging and modeling techniques have been used to create the shadow image. Three independent techniques, namely *eht imaging*, SIMLI, and DIFMAP, estimated the average shadow diameter at $46.9\,\mu$as $\leq \theta_d \leq 50\,\mu$as. The *EHT* observations of SgrA* manifest a

Table 3 Constraints on the parameters a and Θ set by the EHT Results

S No.	ω	M87*		SgrA*	
		a	Θ	a	Θ
1	$-2/3$	0.6167	$0 \leq \Theta \leq 0.004993$	0.7029	$\Theta = 0.005$
2	$-2/3$	0.9627	$0 \leq \Theta \leq 0.0003165$	0.9146	$0.001497 \leq \Theta \leq 0.002868$

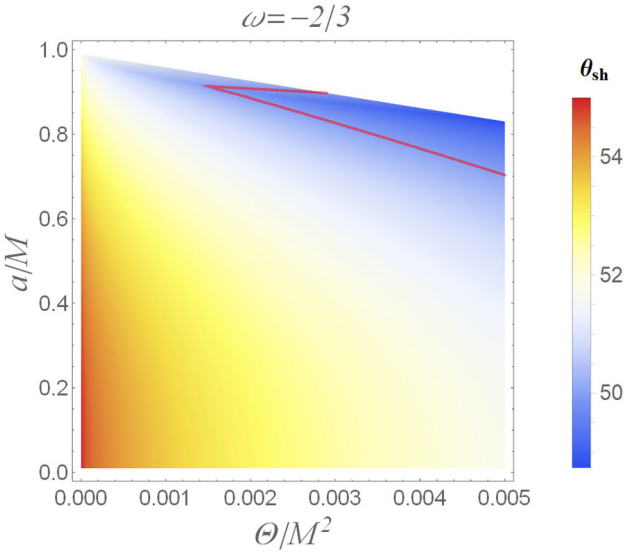

Fig. 8 The angular diameter θ_{sh} of RNKBH shadows is shown as a function of a/M and Θ/M^2 for an inclination angle of $i = 50°$. The red curve indicates $\theta_{sh} = 50\,\mu$as of the SgrA*. The white region is forbidden for $(a/M, \Theta/M^2)$

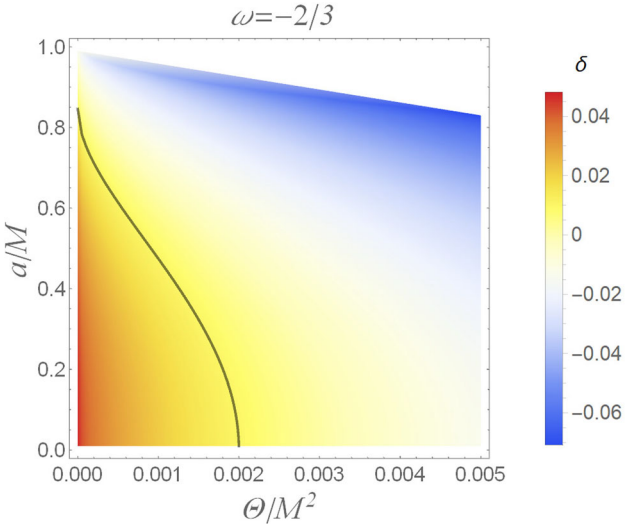

Fig. 9 Plot showing Schwarzschild deviation δ of the RNKBH shadows as a function of a/M and Θ/M^2. The Sgr A* black hole shadow restrictions by EHT are indicated by the black curve at $\delta = 0.01$. The inclination angle is $\theta_0 = 50°$, and the white region is forbidden for $(a/M, \alpha/M^2)$

bright, thick emission ring with a diameter of $51.8 \pm 2.3\,\mu$as, which is consistent with the predictions from black hole mass estimated from stellar dynamics [155], surrounding a brightness dispersion, known as a black hole shadow [80]. The shadow angular diameter, $\theta_d = 2R_a/d$, by employing the RNKBH as a model for SgrA*, has been calculated and represented graphically in Fig. 8, as a function of a and Θ using an inclination angle of $i = 50°$. The red contour line represents the upper bound on $\theta_d = 50\,\mu$as. The area above the contour line is consistent with the observational results of *EHT*. However, in Fig. 8, a lower limit is absent. It is obvious that there is a region that is consistent with the *EHT* results. Surprisingly, the small values Θ are not applicable here. The quantitative analysis of the parameters establishes the upper and lower bounds as shown in Table 3.

Next, we calculate the δ for the SgrA* black hole and impose the limit. The *EHT* applied two independent techniques, namely Keck and VLTI observations, to compute the limits of δ. The reported bounds are $\delta = -0.08^{+0.09}_{-0.09}$ for VLTI and $-0.04^{+0.09}_{-0.10}$ for Keck observation [8,155]. The δ for different cases of ω using the inclination angle of $i = 50°$ has been calculated and represented in Fig. 9. For $\omega = -2/3$, the VLTI bound $(-0.17, 0.01)$ restricts the parameters $(a/M, \Theta/M^2)$ such that for $0.001983 \leq \Theta \leq 0.005$ at $a = 0.01287$ and $0 \leq \Theta \leq 0.005$ at $a = 0.844$. Interestingly, $\delta < -0.075$ and $\delta > 0$ have been observed in Fig. 9, indicates that the current analysis is also valid for non-Kerr black holes.

7 Conclusions

In this work, we analyze the shadows cast by rotating non-commutative Kiselev black holes (RNKBHs) and derive constraints on their parameters using EHT observations of M87* and Sgr A*. The rotating solution was derived using the Newman–Janis algorithm, incorporating non-commutative effects (Θ) and quintessential dark energy (ω). The horizon structure depends on ω: for $\omega = -2/3$, an additional cosmological horizon appears. To avoid naked singularities, Θ must remain small, with critical values depending on ω.

The shadow analysis demonstrated that both the size and shape of RNKBH shadows are influenced by Θ, a, and ω. The shadows become more distorted with increasing inclination angle, with maximum distortion occurring at $i = 90°$. For $\omega = -2/3$, where a cosmological horizon exists, we found that observable shadows only form when the observer is positioned between the photon sphere and the cosmological horizon. The shadow size varies dramatically with the observer's position, shrinking to a point as the observer approaches the cosmological horizon.

Using two independent methodologies – the Hioki and Maeda approach (based on R_s and δ_s) and the Kumar and Ghosh method (using A and D) – we quantitatively estimated the allowed ranges for a and Θ. Both approaches yielded consistent results, with the shadow size decreasing and distortion increasing for larger values of a and Θ. The quintessence parameter ω was found to affect these relationships significantly.

We incorporated the *EHT* observation's results to constrain the parameters by assuming M87* and SgrA* as RNKBH. Two observables, namely, the shadow angular diameter and the Schwarzschild shadow deviation, have been computed quantitatively, and the results obtained are

1. The upper and lower bounds of the parameters were quantitatively estimated and compared with the EHT results for M87*. The bounds obtained are $0 \leq \Theta \leq 0.004993M^2$ at $a = 0.6167$ for $\omega = -2/3$. The angle of inclination is used 17^0.
2. The Schwarzschild shadow deviation $\delta = -0.01 \pm 0.17$ of M87* with an inclination angle of 17^0 was calculated, and it complied with the whole parameter space.
3. The upper and lower bounds have been estimated and compared with the EHT results for SgrA* with an inclination angle of 50^0. For $\omega = -2/3$, at $a = 0.9146$, $0.001497 \leq \Theta \leq 0.002868M^2$.
4. Finally, the Schwarzschild shadow deviation δ has been calculated for SgrA* for different ω with an inclination angle of 50^0. Fascinatingly, we received the bounds as per VLTI observations; however, no upper bound has been observed as per the criteria of the Keck observations. The VLTI bound $(-0.17, 0.01)$ restricts the parameters $(a/M, \Theta/M^2)$ such that for $\omega = -2/3$, $0.001983 \leq \Theta \leq 0.005$ at $a = 0.01287$ and $0 \leq \Theta \leq 0.005$ at $a = 0.844$.

In summary, we have quantified the constraints on the parameters of an RNKBH, and these constraints are consistent with the findings of *EHT* for M87* and SgrA*. Despite this, it is difficult to identify the difference between the shadows of the RNKBHs and those of the standard Kerr black hole by the ongoing measurements. However, we hope to obtain results with better precision soon from the new generation *EHT*, which might help us to ascertain the parameters with greater precision and offer a signature of dark energy.

Acknowledgements F.A. would like to thank Zhejiang University of Technology for the postdoctoral research fellowship. S.G.G. thanks ANRF, India for project No. CRG/2021/005771. F.A., Q.W., and T.Z. are supported by the National Natural Science Foundation of China under Grants No. 12275238 and No. 11675143, the Zhejiang Provincial Natural Science Foundation of China under Grants No. LR21A050001 and No. LY20A050002, the National Key Research and Development Program of China under Grant No. 2020YFC2201503, and the Fundamental Research Funds for the Provincial Universities of Zhejiang in China under Grant No. RF-A2019015.

Funding This work is supported by the National Natural Science Foundation of China under Grants No. 12275238, the Zhejiang Provincial Natural Science Foundation of China under Grants No. LR21A050001 and No. LY20A050002, the National Key Research and Development Program of China under Grant No. 2020YFC2201503, and the Fundamental Research Funds for the Provincial Universities of Zhejiang in China under Grant No. RFA2019015.

Data Availability Statement This manuscript has no associated data. [Author's comment: Data sharing is not applicable to this article, as no datasets were generated or analyzed during the current study.]

Code Availability Statement This manuscript has no associated code/software. [Author's comment: Code/software sharing is not applicable to this article, as no code/software was generated or analyzed during the current study.]

Funded by SCOAP[3].

References

1. B.P. Abbott et al. (LIGO Scientific, Virgo), Phys. Rev. Lett. **116**, 061102 (2016). https://doi.org/10.1103/PhysRevLett.116.061102. arXiv:1602.03837 [gr-qc]
2. B.P. Abbott et al. (LIGO Scientific, Virgo), Phys. Rev. Lett. **116**, 241102 (2016). https://doi.org/10.1103/PhysRevLett.116.241102. arXiv:1602.03840 [gr-qc]
3. B.P. Abbott et al. (LIGO Scientific, Virgo), Phys. Rev. Lett. **116**, 221101 (2016). https://doi.org/10.1103/PhysRevLett.116.221101. arXiv:1602.03841 [gr-qc]. [Erratum: Phys. Rev. Lett. **121**, 129902 (2018)]
4. K. Akiyama et al. (Event Horizon Telescope), ApJL **875**, L1 (2019). https://doi.org/10.3847/2041-8213/ab0ec7. arXiv:1906.11238 [astro-ph.GA]
5. K. Akiyama et al. (Event Horizon Telescope), ApJL **875**, L4 (2019). https://doi.org/10.3847/2041-8213/ab0e85. arXiv:1906.11241 [astro-ph.GA]
6. K. Akiyama et al. (Event Horizon Telescope), ApJL **875**, L6 (2019). https://doi.org/10.3847/2041-8213/ab1141. arXiv:1906.11243 [astro-ph.GA]
7. K. Akiyama et al. (Event Horizon Telescope), Astrophys. J. Lett. **930**, L15 (2022). https://doi.org/10.3847/2041-8213/ac6736
8. K. Akiyama et al. (Event Horizon Telescope), Astrophys. J. Lett. **930**, L17 (2022). https://doi.org/10.3847/2041-8213/ac6756
9. S.E. Gralla, Phys. Rev. D **103**, 024023 (2021). https://doi.org/10.1103/PhysRevD.103.024023. arXiv:2010.08557 [astro-ph.HE]
10. S.H. Völkel, E. Barausse, N. Franchini, A.E. Broderick, Class. Quantum Gravity **38**, 21LT01 (2021). https://doi.org/10.1088/1361-6382/ac27ed. arXiv:2011.06812 [gr-qc]
11. P. Tiede, A.E. Broderick, D.C.M. Palumbo, Astrophys. J. **925**, 122 (2022). https://doi.org/10.3847/1538-4357/ac3a6b. arXiv:2012.07889 [astro-ph.IM]
12. B. Bandyopadhyay, C. Fendt, D.R.G. Schleicher, C. Vourellis, Mon. Not. R. Astron. Soc. **507**, 4933 (2021). https://doi.org/10.1093/mnras/stab2485. arXiv:2102.10735 [astro-ph.HE]
13. P. Kocherlakota et al. (Event Horizon Telescope), Phys. Rev. D **103**, 104047 (2021). https://doi.org/10.1103/PhysRevD.103.104047. arXiv:2105.09343 [gr-qc]

14. A.F. Zakharov, Universe **8**, 141 (2022). https://doi.org/10.3390/universe8030141. arXiv:2108.01533 [gr-qc]
15. J.L. Synge, MNRAS **131**, 463 (1966). https://doi.org/10.1093/mnras/131.3.463
16. J.P. Luminet, A&A **75**, 228 (1979)
17. M. Afrin, S.G. Ghosh, Astrophys. J. **932**, 51 (2022). https://doi.org/10.3847/1538-4357/ac6dda. arXiv:2110.05258 [gr-qc]
18. S.G. Ghosh, R.K. Walia, in *16th Marcel Grossmann Meeting on Recent Developments in Theoretical and Experimental General Relativity, Astrophysics and Relativistic Field Theories* (2022). https://doi.org/10.1142/9789811269776_0084. arXiv:2203.07775 [gr-qc]
19. S.H. Hendi, K. Jafarzade, B. Eslam Panah, JCAP **02**, 022 (2023). https://doi.org/10.1088/1475-7516/2023/02/022. arXiv:2206.05132 [gr-qc]
20. R. Kumar Walia, S.G. Ghosh, S.D. Maharaj, Astrophys. J. **939**, 77 (2022). https://doi.org/10.3847/1538-4357/ac9623. arXiv:2207.00078 [gr-qc]
21. R. Carballo-Rubio, F. Di Filippo, S. Liberati, M. Visser, JCAP **08**, 055 (2022). https://doi.org/10.1088/1475-7516/2022/08/055. arXiv:2205.13555 [astro-ph.HE]
22. H. Falcke, F. Melia, E. Agol, ApJL **528**, L13 (2000). https://doi.org/10.1086/312423. arXiv:astro-ph/9912263
23. A. de Vries, Class. Quantum Gravity **17**, 123 (1999). https://doi.org/10.1088/0264-9381/17/1/309
24. Z.Q. Shen, K.Y. Lo, M.C. Liang, P.T.P. Ho, J.H. Zhao, Nature **438**, 62 (2005). https://doi.org/10.1038/nature04205. arXiv:astro-ph/0512515
25. A. Yumoto, D. Nitta, T. Chiba, N. Sugiyama, Phys. Rev. D **86**, 103001 (2012). https://doi.org/10.1103/PhysRevD.86.103001. arXiv:1208.0635 [gr-qc]
26. F. Atamurotov, A. Abdujabbarov, B. Ahmedov, Phys. Rev. D **88**, 064004 (2013). https://doi.org/10.1103/PhysRevD.88.064004
27. A.A. Abdujabbarov, L. Rezzolla, B.J. Ahmedov, MNRAS **454**, 2423 (2015). https://doi.org/10.1093/mnras/stv2079. arXiv:1503.09054 [gr-qc]
28. P.V.P. Cunha, C.A.R. Herdeiro, Gen. Relativ. Gravit. **50**, 42 (2018). https://doi.org/10.1007/s10714-018-2361-9. arXiv:1801.00860 [gr-qc]
29. R. Kumar, S.G. Ghosh, ApJ **892**, 78 (2020). https://doi.org/10.3847/1538-4357/ab77b0. arXiv:1811.01260 [gr-qc]
30. M. Afrin, S.G. Ghosh, Universe **8**, 52 (2022). https://doi.org/10.3390/universe8010052. arXiv:2112.15038 [gr-qc]
31. K. Hioki, K.-I. Maeda, Phys. Rev. D **80**, 024042 (2009). https://doi.org/10.1103/PhysRevD.80.024042. arXiv:0904.3575 [astro-ph.HE]
32. S. Chen, J. Jing, JCAP **05**, 023 (2024). https://doi.org/10.1088/1475-7516/2024/05/023. arXiv:2310.06490 [gr-qc]
33. X.-Q. Li, H.-P. Yan, X.-J. Yue, S.-W. Zhou, Q. Xu, JCAP **05**, 048 (2024). https://doi.org/10.1088/1475-7516/2024/05/048. arXiv:2401.18066 [gr-qc]
34. A.F. Zakharov (2023). arXiv:2305.15446 [gr-qc]
35. M. Afrin, R. Kumar, S.G. Ghosh, Mon. Not. R. Astron. Soc. **504**, 5927 (2021). https://doi.org/10.1093/mnras/stab1260. arXiv:2103.11417 [gr-qc]
36. R. Kumar, S.G. Ghosh, A. Wang, Phys. Rev. D **100**, 124024 (2019). https://doi.org/10.1103/PhysRevD.100.124024. arXiv:1912.05154 [gr-qc]
37. R. Kumar, S.G. Ghosh, A. Wang, Phys. Rev. D **101**, 104001 (2020). https://doi.org/10.1103/PhysRevD.101.104001. arXiv:2001.00460 [gr-qc]
38. H. Rehman, G. Abbas, T. Zhu, G. Mustafa, Eur. Phys. J. C **83**, 856 (2023). https://doi.org/10.1140/epjc/s10052-023-12033-5. arXiv:2307.16155 [gr-qc]
39. R. Kumar Walia, Phys. Rev. D **110**, 064058 (2024). https://doi.org/10.1103/PhysRevD.110.064058. arXiv:2409.13290 [gr-qc]
40. H.-Y. Shi, T. Zhu, Eur. Phys. J. C **84**, 814 (2024). https://doi.org/10.1140/epjc/s10052-024-13198-3
41. L. Amarilla, E.F. Eiroa, G. Giribet, Phys. Rev. D **81**, 124045 (2010). https://doi.org/10.1103/PhysRevD.81.124045. arXiv:1005.0607 [gr-qc]
42. L. Amarilla, E.F. Eiroa, Phys. Rev. D **85**, 064019 (2012). https://doi.org/10.1103/PhysRevD.85.064019. arXiv:1112.6349 [gr-qc]
43. L. Amarilla, E.F. Eiroa, Phys. Rev. D **87**, 044057 (2013). https://doi.org/10.1103/PhysRevD.87.044057. arXiv:1301.0532 [gr-qc]
44. M. Amir, B.P. Singh, S.G. Ghosh, Eur. Phys. J. C **78**, 399 (2018). https://doi.org/10.1140/epjc/s10052-018-5872-3. arXiv:1707.09521 [gr-qc]
45. B.P. Singh, S.G. Ghosh, Ann. Phys. **395**, 127 (2018). https://doi.org/10.1016/j.aop.2018.05.010. arXiv:1707.07125 [gr-qc]
46. Y. Mizuno, Z. Younsi, C.M. Fromm, O. Porth, M. De Laurentis, H. Olivares, H. Falcke, M. Kramer, L. Rezzolla, Nat. Astron. **2**, 585 (2018). https://doi.org/10.1038/s41550-018-0449-5. arXiv:1804.05812 [astro-ph.GA]
47. A. Allahyari, M. Khodadi, S. Vagnozzi, D.F. Mota, JCAP **02**, 003 (2020). https://doi.org/10.1088/1475-7516/2020/02/003. arXiv:1912.08231 [gr-qc]
48. U. Papnoi, F. Atamurotov, S.G. Ghosh, B. Ahmedov, Phys. Rev. D **90**, 024073 (2014). https://doi.org/10.1103/PhysRevD.90.024073. arXiv:1407.0834 [gr-qc]
49. R. Kumar, S.G. Ghosh, JCAP **07**, 053 (2020). https://doi.org/10.1088/1475-7516/2020/07/053. arXiv:2003.08927 [gr-qc]
50. S.G. Ghosh, R. Kumar, S.U. Islam, JCAP **03**, 056 (2021). https://doi.org/10.1088/1475-7516/2021/03/056. arXiv:2011.08023 [gr-qc]
51. M. Guo, P.-C. Li, Eur. Phys. J. C **80**, 588 (2020). https://doi.org/10.1140/epjc/s10052-020-8164-7. arXiv:2003.02523 [gr-qc]
52. S. Vagnozzi et al., Class. Quantum Gravity **40**, 165007 (2023). https://doi.org/10.1088/1361-6382/acd97b. arXiv:2205.07787 [gr-qc]
53. S. Vagnozzi, L. Visinelli, Phys. Rev. D **100**, 024020 (2019). https://doi.org/10.1103/PhysRevD.100.024020. arXiv:1905.12421 [gr-qc]
54. X.-J. Gao, T.-T. Sui, X.-X. Zeng, Y.-S. An, Y.-P. Hu, Eur. Phys. J. C **83**, 1052 (2023). https://doi.org/10.1140/epjc/s10052-023-12231-1. arXiv:2311.11780 [gr-qc]
55. S. Li, T. Mirzaev, A.A. Abdujabbarov, D. Malafarina, B. Ahmedov, W.-B. Han, Phys. Rev. D **106**, 084041 (2022). https://doi.org/10.1103/PhysRevD.106.084041. arXiv:2207.10933 [gr-qc]
56. I. Sengo, P.V.P. Cunha, C.A.R. Herdeiro, E. Radu, JCAP **01**, 047 (2023). https://doi.org/10.1088/1475-7516/2023/01/047. arXiv:2209.06237 [gr-qc]
57. W. Liu, D. Wu, X. Fang, J. Jing, J. Wang, JCAP **08**, 035 (2024). https://doi.org/10.1088/1475-7516/2024/08/035. arXiv:2406.00579 [gr-qc]
58. M. Afrin, S.G. Ghosh, A. Wang, Phys. Dark Universe **46**, 101642 (2024). https://doi.org/10.1016/j.dark.2024.101642. arXiv:2409.06218 [gr-qc]
59. K. Jafarzade, S.H. Hendi, M. Jamil, S. Bahamonde, Phys. Dark Universe **45**, 101497 (2024). https://doi.org/10.1016/j.dark.2024.101497. arXiv:2309.02454 [gr-qc]
60. C. Liu, S. Yang, Q. Wu, T. Zhu, JCAP **02**, 034 (2022). https://doi.org/10.1088/1475-7516/2022/02/034. arXiv:2107.04811 [gr-qc]
61. C. Liu, T. Zhu, Q. Wu, Chin. Phys. C **45**, 015105 (2021). https://doi.org/10.1088/1674-1137/abc16c. arXiv:2004.01662 [gr-qc]
62. T. Zhu, Q. Wu, M. Jamil, K. Jusufi, Phys. Rev. D **100**, 044055 (2019). https://doi.org/10.1103/PhysRevD.100.044055. arXiv:1906.05673 [gr-qc]
63. F. Ahmed, S.U. Islam, S.G. Ghosh, JHEAp **46**, 100350 (2025). https://doi.org/10.1016/j.jheap.2025.100350

64. M. Khodadi, E.N. Saridakis, Phys. Dark Universe **32**, 100835 (2021). https://doi.org/10.1016/j.dark.2021.100835. arXiv:2012.05186 [gr-qc]
65. M. Khodadi, G. Lambiase, Phys. Rev. D **106**, 104050 (2022). https://doi.org/10.1103/PhysRevD.106.104050. arXiv:2206.08601 [gr-qc]
66. M. Khodadi, Nucl. Phys. B **985**, 116014 (2022). https://doi.org/10.1016/j.nuclphysb.2022.116014. arXiv:2211.00300 [gr-qc]
67. M. Khodadi, S. Vagnozzi, J.T. Firouzjaee, Sci. Rep. **14**, 26932 (2024). https://doi.org/10.1038/s41598-024-78264-y. arXiv:2408.03241 [gr-qc]
68. B.P. Singh, R. Kumar, S.G. Ghosh, New Astron. **99**, 101945 (2023). https://doi.org/10.1016/j.newast.2022.101945
69. Y. Hou, M. Guo, B. Chen, Phys. Rev. D **104**, 024001 (2021). https://doi.org/10.1103/PhysRevD.104.024001. arXiv:2103.04369 [gr-qc]
70. S. Vagnozzi, L. Visinelli, Res. Notes AAS **6**, 106 (2022). https://doi.org/10.3847/2515-5172/ac7331. arXiv:2205.11314 [astro-ph.GA]
71. I. Banerjee, S. Chakraborty, S. SenGupta, Phys. Rev. D **106**, 084051 (2022). https://doi.org/10.1103/PhysRevD.106.084051. arXiv:2207.09003 [gr-qc]
72. A.S. Lemos, J.A.V. Campos, F.A. Brito, Phys. Rev. D **110**, 064079 (2024). https://doi.org/10.1103/PhysRevD.110.064079. arXiv:2407.04609 [gr-qc]
73. F. Ahmed, D.V. Singh, S.G. Ghosh, Gen. Relativ. Gravit. **54**, 21 (2022). https://doi.org/10.1007/s10714-022-02906-7. arXiv:2002.12031 [gr-qc]
74. T. Johannsen, D. Psaltis, ApJ **718**, 446 (2010). https://doi.org/10.1088/0004-637X/718/1/446. arXiv:1005.1931 [astro-ph.HE]
75. T. Baker, D. Psaltis, C. Skordis, Astrophys. J. **802**, 63 (2015). https://doi.org/10.1088/0004-637X/802/1/63. arXiv:1412.3455 [astro-ph.CO]
76. A.E. Broderick, T. Johannsen, A. Loeb, D. Psaltis, Astrophys. J. **784**, 7 (2014). https://doi.org/10.1088/0004-637X/784/1/7. arXiv:1311.5564 [astro-ph.HE]
77. M. Khodadi, A. Allahyari, S. Vagnozzi, D.F. Mota, JCAP **09**, 026 (2020). https://doi.org/10.1088/1475-7516/2020/09/026. arXiv:2005.05992 [gr-qc]
78. M. Khodadi, G. Lambiase, D.F. Mota, JCAP **09**, 028 (2021). https://doi.org/10.1088/1475-7516/2021/09/028. arXiv:2107.00834 [gr-qc]
79. K. Glampedakis, G. Pappas, Phys. Rev. D **107**, 064001 (2023). https://doi.org/10.1103/PhysRevD.107.064001. arXiv:2302.06140 [gr-qc]
80. M. Afrin, S. Vagnozzi, S.G. Ghosh, Astrophys. J. **944**, 149 (2023). https://doi.org/10.3847/1538-4357/acb334. arXiv:2209.12584 [gr-qc]
81. S.U. Islam, J. Kumar, R. Kumar Walia, S.G. Ghosh, Astrophys. J. **943**, 22 (2023). https://doi.org/10.3847/1538-4357/aca411. arXiv:2211.06653 [gr-qc]
82. S.G. Ghosh, M. Afrin, Astrophys. J. **944**, 174 (2023). https://doi.org/10.3847/1538-4357/acb695. arXiv:2206.02488 [gr-qc]
83. S.G. Ghosh, Eur. Phys. J. C **76**, 222 (2016). https://doi.org/10.1140/epjc/s10052-016-4051-7. arXiv:1512.05476 [gr-qc]
84. L. Modesto, P. Nicolini, Phys. Rev. D **82**, 104035 (2010). https://doi.org/10.1103/PhysRevD.82.104035. arXiv:1005.5605 [gr-qc]
85. M. Visser, Class. Quantum Gravity **37**, 045001 (2020). https://doi.org/10.1088/1361-6382/ab60b8. arXiv:1908.11058 [gr-qc]
86. A. Uniyal, R.C. Pantig, A. Övgün, Phys. Dark Universe **40**, 101178 (2023). https://doi.org/10.1016/j.dark.2023.101178. arXiv:2205.11072 [gr-qc]
87. R.C. Pantig, A. Övgün, Ann. Phys. **448**, 169197 (2023). https://doi.org/10.1016/j.aop.2022.169197. arXiv:2206.02161 [gr-qc]
88. C. Liu, T. Zhu, Q. Wu, K. Jusufi, M. Jamil, M. Azreg-Aïnou, A. Wang, Phys. Rev. D **101**, 084001 (2020). https://doi.org/10.1103/PhysRevD.101.084001. arXiv:2003.00477 [gr-qc]. [Erratum: Phys. Rev. D **103**, 089902 (2021)]
89. S. Brahma, C.-Y. Chen, D.-H. Yeom, Phys. Rev. Lett. **126**, 181301 (2021). https://doi.org/10.1103/PhysRevLett.126.181301. arXiv:2012.08785 [gr-qc]
90. R. Kumar Walia, JCAP **03**, 029 (2023). https://doi.org/10.1088/1475-7516/2023/03/029. arXiv:2207.02106 [gr-qc]
91. J. Yang, C. Zhang, Y. Ma, Eur. Phys. J. C **83**, 619 (2023). https://doi.org/10.1140/epjc/s10052-023-11800-8. arXiv:2211.04263 [gr-qc]
92. H.-X. Jiang, C. Liu, I.K. Dihingia, Y. Mizuno, H. Xu, T. Zhu, Q. Wu, JCAP **01**, 059 (2024). https://doi.org/10.1088/1475-7516/2024/01/059. arXiv:2312.04288 [gr-qc]
93. H.-X. Jiang, I.K. Dihingia, C. Liu, Y. Mizuno, T. Zhu, JCAP **05**, 101 (2024). https://doi.org/10.1088/1475-7516/2024/05/101. arXiv:2402.08402 [astro-ph.HE]
94. C. Ni, A.E. Broderick, R. Gold, Astrophys. J. **940**, 149 (2022). https://doi.org/10.3847/1538-4357/ac9b47. arXiv:2212.02544 [astro-ph.IM]
95. L. Medeiros, D. Psaltis, T.R. Lauer, F. Ozel, Astrophys. J. **943**, 144 (2023). https://doi.org/10.3847/1538-4357/acaa9a. arXiv:2208.01667 [astro-ph.HE]
96. J. Kumar, S.U. Islam, S.G. Ghosh, Eur. Phys. J. C **82**, 443 (2022). https://doi.org/10.1140/epjc/s10052-022-10357-2. arXiv:2109.04450 [gr-qc]
97. J. Kumar, S.U. Islam, S.G. Ghosh, Eur. Phys. J. C **83**, 1014 (2023). https://doi.org/10.1140/epjc/s10052-023-12205-3. arXiv:2305.04336 [gr-qc]
98. P. Boonserm, S. Phalungsongsathit, K. Sansuk, P. Wongjun, Eur. Phys. J. C **83**, 657 (2023). https://doi.org/10.1140/epjc/s10052-023-11843-x. arXiv:2305.00459 [gr-qc]
99. K. Nozari, S. Saghafi, Eur. Phys. J. C **83**, 588 (2023). https://doi.org/10.1140/epjc/s10052-023-11755-w. arXiv:2305.17237 [gr-qc]
100. R. Kumar, B.P. Singh, M.S. Ali, S.G. Ghosh, Phys. Dark Universe **34**, 100881 (2021). https://doi.org/10.1016/j.dark.2021.100881. arXiv:1712.09793 [gr-qc]
101. B.P. Singh, Ann. Phys. **441**, 168892 (2022). https://doi.org/10.1016/j.aop.2022.168892. arXiv:1711.02898 [gr-qc]
102. A. Övgün, L.J.F. Sese, R.C. Pantig, Ann. Phys. **536**, 2300390 (2024). https://doi.org/10.1002/andp.202300390. arXiv:2309.07442 [gr-qc]
103. M. Zubair, M.A. Raza, E. Maqsood, Phys. Dark Universe **42**, 101334 (2023). https://doi.org/10.1016/j.dark.2023.101334. arXiv:2310.12325 [gr-qc]
104. S. Capozziello, S. Zare, H. Hassanabadi (2023). arXiv:2311.12896 [gr-qc]
105. V.V. Kiselev, Class. Quantum Gravity **20**, 1187 (2003). https://doi.org/10.1088/0264-9381/20/6/310. arXiv:gr-qc/0210040
106. S.-B. Chen, J.-L. Jing, Class. Quantum Gravity **22**, 4651 (2005). https://doi.org/10.1088/0264-9381/22/21/011. arXiv:gr-qc/0511085
107. Y. Zhang, Y.X. Gui, Class. Quantum Gravity **23**, 6141 (2006). https://doi.org/10.1088/0264-9381/23/22/004. arXiv:gr-qc/0612009
108. S. Chen, B. Wang, R. Su, Phys. Rev. D **77**, 124011 (2008). https://doi.org/10.1103/PhysRevD.77.124011. arXiv:0801.2053 [gr-qc]
109. Y.-H. Wei, Z.-H. Chu, Chin. Phys. Lett. **28**, 100403 (2011). https://doi.org/10.1088/0256-307X/28/10/100403
110. B.B. Thomas, M. Saleh, T.C. Kofane, Gen. Relativ. Gravit. **44**, 2181 (2012). https://doi.org/10.1007/s10714-012-1382-z. arXiv:1604.06207 [gr-qc]
111. Z. Xu, J. Wang, Phys. Rev. D **95**, 064015 (2017). https://doi.org/10.1103/PhysRevD.95.064015. arXiv:1609.02045 [gr-qc]

112. J. de Oliveira, R.D.B. Fontana, Phys. Rev. D **98**, 044005 (2018). https://doi.org/10.1103/PhysRevD.98.044005. arXiv:1804.00210 [gr-qc]
113. K. Nozari, M. Hajebrahimi, S. Saghafi, Eur. Phys. J. C **80**, 1208 (2020). https://doi.org/10.1140/epjc/s10052-020-08782-2. arXiv:2101.05054 [gr-qc]
114. S.G. Ghosh, M. Amir, S.D. Maharaj, Eur. Phys. J. C **77**, 530 (2017). https://doi.org/10.1140/epjc/s10052-017-5099-8. arXiv:1611.02936 [gr-qc]
115. B. Hamil, B.C. Lütfüoğlu, Phys. Dark Universe **44**, 101484 (2024). https://doi.org/10.1016/j.dark.2024.101484. arXiv:2401.09295 [gr-qc]
116. P. Nicolini, A. Smailagic, E. Spallucci, Phys. Lett. B **632**, 547 (2006). https://doi.org/10.1016/j.physletb.2005.11.004. arXiv:gr-qc/0510112
117. P.R. Giri, Int. J. Mod. Phys. A **22**, 2047 (2007). https://doi.org/10.1142/S0217751X07036245. arXiv:hep-th/0604188
118. M.A. Anacleto, F.A. Brito, J.A.V. Campos, E. Passos, Phys. Lett. B **803**, 135334 (2020). https://doi.org/10.1016/j.physletb.2020.135334. arXiv:1907.13107 [hep-th]
119. P. Nicolini, Bled Workshops Phys. **6**, 79 (2005). arXiv:hep-th/0510203
120. R. Kumar, S.G. Ghosh, Eur. Phys. J. C **77**, 577 (2017). https://doi.org/10.1140/epjc/s10052-017-5141-x. arXiv:1703.10479 [gr-qc]
121. S.G. Ghosh, Class. Quantum Gravity **35**, 085008 (2018). https://doi.org/10.1088/1361-6382/aaaead. arXiv:1707.08174 [gr-qc]
122. S.G. Ghosh, S.D. Maharaj, Phys. Dark Universe **31**, 100793 (2021). https://doi.org/10.1016/j.dark.2021.100793. arXiv:2004.13519 [gr-qc]
123. E.T. Newman, A.I. Janis, J. Math. Phys. **6**, 915 (1965). https://doi.org/10.1063/1.1704350
124. R. Penrose, R.M. Floyd, Nature **229**, 177 (1971). https://doi.org/10.1038/physci229177a0
125. B. Carter, Phys. Rev. **174**, 1559 (1968). https://doi.org/10.1103/PhysRev.174.1559
126. S. Chandrasekhar, *The Mathematical Theory of Black Holes* (Oxford University Press, New York, 1985)
127. V.P. Frolov, A. Zelnikov, *Introduction to Black Hole Physics* (Oxford University Press, Oxford, 2011)
128. D.C. Wilkins, Phys. Rev. D **5**, 814 (1972). https://doi.org/10.1103/PhysRevD.5.814
129. H. Goldstein, Z. Phys. **271**, 275 (1974). https://doi.org/10.1007/BF01677935
130. M. Johnston, R. Ruffini, Phys. Rev. D **10**, 2324 (1974). https://doi.org/10.1103/PhysRevD.10.2324
131. S.V. Izmailov, E.S. Levin, Izvestiya Vysshikh Uchebnykh Zavedenij, Fizika, 17 (1979). http://inis.iaea.org/search/search.aspx?orig_q=RN:11503300
132. S.V. Izmailov, E.S. Levin, Sov. Phys. J. **23**, 645 (1980). https://doi.org/10.1007/BF00891345
133. E. Teo, Gen. Relativ. Gravit. **53**, 10 (2021). https://doi.org/10.1007/s10714-020-02782-z. arXiv:2007.04022 [gr-qc]
134. J.M. Bardeen, J.A. Petterson, ApJL **195**, L65 (1975). https://doi.org/10.1086/181711
135. J.M. Bardeen, W.H. Press, S.A. Teukolsky, ApJ **178**, 347 (1972). https://doi.org/10.1086/151796
136. K.S. Virbhadra, G.F.R. Ellis, Phys. Rev. D **62**, 084003 (2000). https://doi.org/10.1103/PhysRevD.62.084003. arXiv:astro-ph/9904193
137. V. Bozza, S. Capozziello, G. Iovane, G. Scarpetta, Gen. Relativ. Gravit. **33**, 1535 (2001). https://doi.org/10.1023/A:1012292927358. arXiv:gr-qc/0102068
138. V. Bozza, Phys. Rev. D **66**, 103001 (2002). https://doi.org/10.1103/PhysRevD.66.103001. arXiv:gr-qc/0208075
139. R. Kumar, S.U. Islam, S.G. Ghosh, Eur. Phys. J. C **80**, 1128 (2020). https://doi.org/10.1140/epjc/s10052-020-08606-3. arXiv:2004.12970 [gr-qc]
140. S.U. Islam, R. Kumar, S.G. Ghosh, JCAP **09**, 030 (2020). https://doi.org/10.1088/1475-7516/2020/09/030. arXiv:2004.01038 [gr-qc]
141. S.U. Islam, S.G. Ghosh, S.D. Maharaj, Chin. J. Phys. **89**, 1710 (2024). https://doi.org/10.1016/j.cjph.2024.03.044. arXiv:2203.00957 [gr-qc]
142. T. Johannsen, ApJ **777**, 170 (2013). https://doi.org/10.1088/0004-637X/777/2/170. arXiv:1501.02814 [astro-ph.HE]
143. A. Grenzebach, V. Perlick, C. Lämmerzahl, Phys. Rev. D **89**, 124004 (2014). https://doi.org/10.1103/PhysRevD.89.124004. arXiv:1403.5234 [gr-qc]
144. P.V.P. Cunha, C.A.R. Herdeiro, M.J. Rodriguez, Phys. Rev. D **97**, 084020 (2018). https://doi.org/10.1103/PhysRevD.97.084020. arXiv:1802.02675 [gr-qc]
145. Y. Huang, Y.-P. Dong, D.-J. Liu, Int. J. Mod. Phys. D **27**, 1850114 (2018). https://doi.org/10.1142/S0218271818501146. arXiv:1807.06268 [gr-qc]
146. P.V.P. Cunha, C.A.R. Herdeiro, E. Radu, Universe **5**, 220 (2019). https://doi.org/10.3390/universe5120220. arXiv:1909.08039 [gr-qc]
147. I. Banerjee, S. Chakraborty, S. SenGupta, Phys. Rev. D **101**, 041301 (2020). https://doi.org/10.1103/PhysRevD.101.041301. arXiv:1909.09385 [gr-qc]
148. S. Vagnozzi, C. Bambi, L. Visinelli, Class. Quantum Gravity **37**, 087001 (2020). https://doi.org/10.1088/1361-6382/ab7965. arXiv:2001.02986 [gr-qc]
149. K. Jusufi, M. Azreg-Aïnou, M. Jamil, E.N. Saridakis, Universe **8**, 102 (2022). https://doi.org/10.3390/universe8020102. arXiv:2110.07258 [gr-qc]
150. Y. Chen, R. Roy, S. Vagnozzi, L. Visinelli, Phys. Rev. D **106**, 043021 (2022). https://doi.org/10.1103/PhysRevD.106.043021. arXiv:2205.06238 [astro-ph.HE]
151. S.G. Ghosh, M. Amir, S.D. Maharaj, Nucl. Phys. B **957**, 115088 (2020). https://doi.org/10.1016/j.nuclphysb.2020.115088. arXiv:2006.07570 [gr-qc]
152. O.Y. Tsupko, Phys. Rev. D **95**, 104058 (2017). https://doi.org/10.1103/PhysRevD.95.104058. arXiv:1702.04005 [gr-qc]
153. N. Tsukamoto, Z. Li, C. Bambi, JCAP **06**, 043 (2014). https://doi.org/10.1088/1475-7516/2014/06/043. arXiv:1403.0371 [gr-qc]
154. J. Schee, Z. Stuchlik, Int. J. Mod. Phys. D **18**, 983 (2009). https://doi.org/10.1142/S0218271809014881. arXiv:0810.4445 [astro-ph]
155. K. Akiyama et al. (Event Horizon Telescope), Astrophys. J. Lett. **930**, L12 (2022). https://doi.org/10.3847/2041-8213/ac6674
156. R. Craig Walker, P.E. Hardee, F.B. Davies, C. Ly, W. Junor, ApJ **855**, 128 (2018). https://doi.org/10.3847/1538-4357/aaafcc. arXiv:1802.06166 [astro-ph.HE]
157. K. Akiyama et al. (Event Horizon Telescope), Astrophys. J. Lett. **875**, L1 (2019). https://doi.org/10.3847/2041-8213/ab0ec7. arXiv:1906.11238 [astro-ph.GA]
158. I. Banerjee, S. Sau, S. SenGupta (2022). arXiv:2207.06034 [gr-qc]
159. H. Ali, S.U. Islam, S.G. Ghosh, JHEAp **47**, 100367 (2025). https://doi.org/10.1016/j.jheap.2025.100367. arXiv:2410.09198 [gr-qc]
160. R. Abuter et al. (Gravity), Astron. Astrophys. **625** (2019). https://doi.org/10.1051/0004-6361/201935656. arXiv:1904.05721 [astro-ph.GA]
161. R. Abuter et al. (GRAVITY), Astron. Astrophys. **645**, A127 (2021). https://doi.org/10.1051/0004-6361/202039544. arXiv:2011.03058 [astro-ph.GA]
162. R. Abuter et al. (GRAVITY), Astron. Astrophys. **657**, L12 (2022). https://doi.org/10.1051/0004-6361/202142465. arXiv:2112.07478 [astro-ph.GA]